1985ApJ...289..732G

THE ASTROPHYSICAL JOURNAL, 289:732–747, 1985 February 15
© 1985. The American Astronomical Society. All rights reserved. Printed in U.S.A.

EMISSION LINES IN THE MAGNETIC WHITE DWARF GD 356

JESSE L. GREENSTEIN AND JAMES K. MCCARTHY
Palomar Observatory, California Institute of Technology
Received 1984 July 16; accepted 1984 August 30

ABSTRACT

GD 356 (1639+53, Gr 329) is a unique white dwarf showing the resolved Zeeman triplets of Hα and Hβ as emission lines. Multichannel spectrophotometry suggests $M_V = +13.3$. Measurements made at high signal-to-noise ratio with the double-spectrograph and CCD detectors at the Hale reflector are presented and analyzed. Multichannel information gives the temperature as 7500 K; any red companion must be fainter than $M_V = +15$. The Balmer decrement is flat, with Hβ apparently stronger than Hα. Modeling the emission region with an extended dipole magnetic field proves unsatisfactory; the radial dependence of field strength in a large emitting region predicts lines wider than observed. The flat decrement suggests that the emission-line region has high density ($N_e \approx 10^{14}$ cm^{-3}) and is optically thick in Lyα. Its radial extent must be small; i.e., it is a chromosphere rather than a corona. If a dipole were present, $B_p \approx 20$ megagauss (MG). A reasonable fit to the emission-line profile is also given by a small-scale random distribution of fields, with mean of roughly 11 MG and dispersion of 1.1 MG.

We study, in passing, the Hα absorption triplet in G99-47 (0553+05, Gr 290), a cooler magnetic degenerate, and use it to correct the emission in GD 356. The Zeeman splitting is even larger (570 Å) than in GD 356 (445 Å). Variation of field with magnetic latitude in a dipole gives excess line broadening. Since the absorption lines are nearly symmetric, the profiles fit a small-scale random field distribution with mean of 14 MG and dispersion of 1.4 MG.

We assume that similar absorption lines underly the emission in GD 356. After scaling the absorption lines in G99-47 to the field in GD 356, the corrected Hα emission is increased by about 50%. The final Hα profile is represented by random fields of 11.2 MG with a spread of 1.1 MG. The observed ratio of fluxes $f(\mathrm{H}\alpha)/f(\mathrm{H}\beta)$ was 0.7; after this correction, it is 1.2. The shallow decrement requires a high-density chromosphere but will not be fully understood until Lyα is measured.

We speculate as to why GD 356 is the only apparently single magnetic white dwarf known with emission lines. No polarization has yet been detected. The following possibilities are discussed: (*a*) An interacting companion exists (although there is no recorded light variability nor any observed X-rays). (*b*) Active convection interacts with the magnetic field to produce magnetoionic heating. Velocities in the chromosphere could be near-relativistic in our models. (*c*) There is ongoing accretion of interstellar matter.

Assuming the distance of GD 356 to be 20 pc, the luminosity in Hα is roughly 2×10^{27} ergs s^{-1}. We address the question of the correct distance, which has important consequences. Since Lyα is optically thick, the electron temperature of the chromosphere affects its visibility even more critically than does the correct distance. We suggest that Lyα emission may be detectable with the *IUE*.

Subject headings: stars: individual — stars: magnetic — stars: white dwarfs

I. INTRODUCTION

The 15th magnitude white dwarf GD 356 (Gr 329, 1639+53) was recently found to show weak emission-line Zeeman triplets at Hα and Hβ (Greenstein 1983; McCarthy and Greenstein 1983). It is the only known (apparently) single white dwarf to have emission lines in a strong magnetic field, i.e., in a chromosphere or corona. Four low-resolution multichannel spectrophotometric scans (MCSP) with the Hale 5 meter reflector (§ II) had shown it to have a nearly continuous spectrum with a suggestion of "roughness" in 1973–1974. This roughness was the reason for taking the four higher resolution, high signal-to-noise observations with the Hale reflector's double CCD spectrograph in 1982 (with the help of Noel Dolez), presented in § III. J. B. Oke and W. L. W. Sargent kindly provided later CCD spectra which confirmed the constancy of the Zeeman structure over a year's interval. The MCSP calibration of white dwarfs (Greenstein 1984) gave GD 356 the type DC7EH; from the normal color-luminosity relation, $M_V = +13.34$. The double CCD spectra have a resolution sufficient to establish that the magnetic field strength is between 10 and 20 megagauss (MG), and that the emitting region is small. A finding chart is given by Giclas, Burnham, and Thomas (1967); their proper-motion class is μ_3 in 225° (corresponding to $0''.20 < \mu < 0''.26$). This motion agrees well with a later value by Luyten (1979); he renames it LP137-43 and finds $\mu = 0''.24$ in 212°.

To our knowledge GD 356 is not a binary, variable star, or radio or X-ray source. The last, and important, point is based on information from F. D. Seward, of the Center for Astrophysics, who finds no X-ray source at the star's position in *Einstein* field 8351, a good exposure centered on an Abell cluster. The X-ray signal is estimated as less than 10^{-13} ergs cm^{-2} s^{-1}. If we assume the X-ray spectrum is flat, an upper limit on the flux is 10^{-31} ergs cm^{-2} s^{-1} Hz^{-1}, i.e., 10^{-5} mJy. The optical flux corresponds to 4 mJy; the spectrum of GD 356 drops steeply toward the high-energy region. Deeper X-ray observations would be valuable. If we assume the X-ray spectrum to be soft, centered at 500 eV, the upper limit to the flux gives a power law steeper than $\nu^{-2.2}$. The optical spectrum fits an 8000 K blackbody or a 7500 K hydrogen model atmosphere. So far, then, no evidence exists, except for the emission

© American Astronomical Society • Provided by the NASA Astrophysics Data System

1985ApJ...289..732G

lines, for a high-temperature component or any nonthermal phenomena.

There is only one continuum-polarization measurement, with a negative result (by Angel, Borra, and Landstreet 1981). The star deserves more detailed polarization measurements; the field we suggest for the emission-line region, if it exists in the region forming the continuum, would produce measurable polarization. A search for rapid light variability should also be carried out.

Can the star be other than a white dwarf, e.g., an accretion disk or an AM Her star? Because of the large Zeeman shifts, the intrinsic radial velocity is not reliable but is certainly not as large or variable as in SS 433. We determine the tangential motion V_T from the absolute magnitude (assuming the MCSP calibration of M_V from color applies),

$$M_V = m_V + 8.39 + 5 \log \mu - 5 \log V_T . \quad (1)$$

We find $V_T = 25$ km s^{-1}, about half the V_T (~ 50 km s^{-1}) of typical old-disk white dwarf space motions. Reversing the process, assume an upper limit to the space motion $V_T \leq 250$ km s^{-1}; then $M_V \geq +8.4$. An accretion disk in an interacting but quiescent system could have such a luminosity. The MCSP data in the red permit us to search for a late-type companion; while nothing suggests that the star is in a binary system, the hypothesis is not excluded and will be explored. The analysis of the physical properties of the emission-line region is in § V.

II. MULTICHANNEL SPECTROPHOTOMETRY

Four MCSP outputs were available from 1973 and 1974; they agree well—with the exception of one, which is 0.13 mag fainter than the mean. That output was obtained with too small an aperture (4″ in good seeing) and so was corrected by −0.13 mag. The original magnitudes on the AB69 scale were updated to AB79 by the AB79 − AB69 correction of Oke and Gunn (1983) for each standard used on the individual nights. The MCSP were rebinned and the means, m_v are plotted in Figure 1 as a function of $1/\lambda$ in μm^{-1}. (We hereafter omit the units for $1/\lambda$.) Also shown at selected wavelengths are the 2 σ errors of the means. Photon statistics are such that most 2 σ errors should be near 0.02, but they can be larger (~ 0.10) in the ultraviolet and infrared. Given the weakness and Zeeman shifts of the emission lines, they should be, and indeed are, only marginally visible in the MCSP data. In Figure 1 the large open circles are the fluxes for a cool hydrogen atmosphere at 8000 K, $\log g = 8$, from Shipman (1977). The zero point is arbitrary; a temperature of 7500 K would be preferable, but Shipman's next cooler published model is at 6000 K. A small Balmer absorption continuum appears both in the model and in the data; a mixed-composition model with moderate He/H ratio would also fit. No absorption lines of He I or He II are visible in our higher resolution CCD spectra.

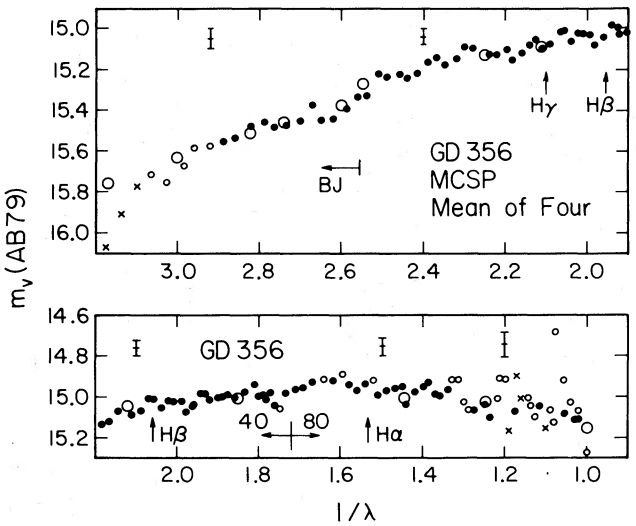


FIG. 1.—The mean multichannel spectrum of GD 356 from four nights in 1973 and 1974. The resolution is 40 Å in the blue, 80 Å in the red. Hydrogen emission is marginally visible, and a weak Balmer absorption continuum also appears. The large open circles are theoretical fluxes from Shipman's hydrogen model at 8000 K, $\log g = 8$ (which does not include the depression by absorption lines). Filled circles indicate good data, open circles fair, crosses discordant means. Vertical bars are 2 σ errors. Ordinate $1/\lambda$ in inverse microns.

Model fluxes are given only at 12 wavelengths, and the absorption lines were not included; detailed comparison with the 120 data points would involve elaborate interpolation. The smoothness of fluxes in the model suggests that comparison of the data with a blackbody would be equally informative. In Greenstein and Oke (1982), white dwarf fluxes were fitted to a blackbody by least squares; the solid angle is derived from the mean offset, $\langle \log \gamma(v, T) \rangle$. Consequently, we take the ratios of the observed GD 356 fluxes to a blackbody, form the magnitude differences, and add a constant for best fit. We omit the least squares test and instead try two plausible temperatures. Figure 2 shows the residuals on an enlarged scale for 8000 K; the symbols indicate the internal observational errors. Hα and Hβ emission is indicated, and higher Balmer lines may be present if the T is as low as 8000 K; with a blackbody at 8300 K, the baseline is slightly rotated, and there is less evidence for the higher lines. There is a Balmer continuum depression at $1/\lambda \geq 2.5$. Greenstein and Oke (1982) found the ratio of blackbody color temperature to effective temperature in a model atmosphere to be near 1.1; this confirms our estimate that the effective temperature of GD 356 is near 7500 K.

The observed fluxes leave little room for a cool main-sequence companion. Let us assume that the system is composite, containing a faint main-sequence dM star and an accretion disk of luminosity $M(1.88) = +8.34$ with a flat optical spectrum (the upper limit from the space motion). J. L. G.'s ongoing study of K and M dwarfs of known parallax gives the following relations between color indices and luminosity:

$$M(1.88) = +4.1 + 2.4[m(2.14) - m(1.20)] , \quad (2)$$

$$[M(1.88) - M(1.10)] = -0.13 + 0.87[M(2.14) - M(1.20)] . \quad (3)$$

Equation (3) is a color-color relation written here in absolute magnitudes to predict the near-infrared luminosity corresponding to an assumed color and visual luminosity from equation (2). The companion is so faint that we can neglect its contribution at 1.88. Assuming the modulus (6.76 for this case) determines the upturn at 1.10 obtained from adding the flux from the dM to that from the assumed flat disk. The slope of an M dwarf energy distribution is so steep that an estimate of the upper limit to the infrared upturn (see Fig. 2) sets a strong limit on the light from any possible dM. Combining equations (2) and (3) gives

$$M(1.10) = 0.64M(1.88) + 1.61 . \quad (4)$$

Assume that all the light at 1.88 arises from the brightest possible accretion disk, with $M_V = +8.34$. Then the brightening at 1.10, $\Delta m(1.10)$, is −0.19 if the dM has

© American Astronomical Society • Provided by the NASA Astrophysics Data System

1985ApJ...289..732G

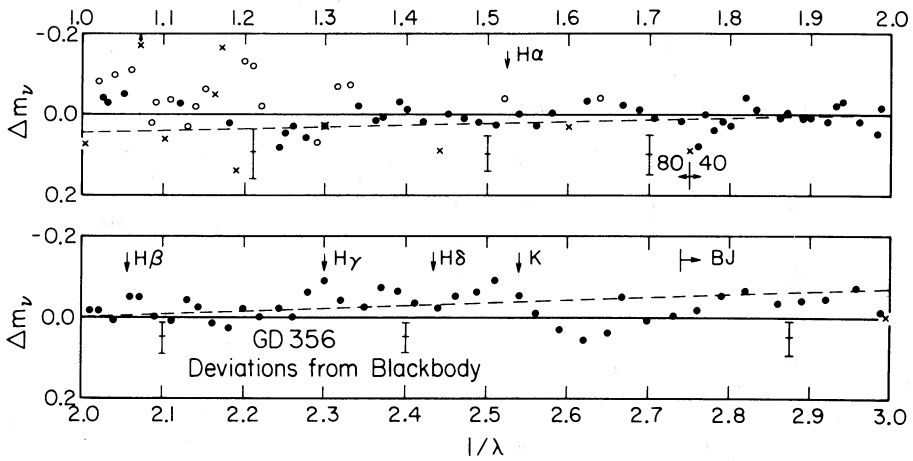


FIG. 2.—The brightness differences between GD 356 and a blackbody at 8000 K; weak emission is marginally visible, as is an apparent Balmer absorption continuum shortward of 4000 Å. Comparison with an 8300 K blackbody would give the deviations as measured from the dashed line—i.e., weaker Balmer emission and larger Balmer jump. The symbols are as in Fig. 1.

$M(1.88) = 13.34$; $\Delta m = -0.10$ at $M(1.88) = 14.49$; $\Delta m = -0.05$ at $M(1.88) = 15.83$; and $\Delta m = -0.02$ if $M(1.88) = 18.34$. Any upturn seen at 1.10 is negligible, so that the dM must be definitely fainter than $M(1.88) = +15$. Such an estimate is only indicative; cataclysmic variables studied with the MCSP rarely show an infrared upturn (Oke and Wade 1982). Only the active cataclysmic variable U Gem, which has a faint disk at minimum light ($M \approx +10$), shows a clear upturn caused by its relatively bright dM companion (see Wade 1979). Incidentally, we cannot blame the Hα emission we see on the active chromosphere of a dMe companion, since Zeeman splitting is negligibly small in the maximum field possible in a stable main-sequence star. We also do not see any single Hα line ascribable to the chromosphere of a dMe.

III. THE DOUBLE CCD SPECTROGRAPH DATA

Four spectra were taken in 1982 with the Cassegrain double spectrograph (DBSP) of the Hale 5 meter reflector; the dispersion used gave 6 Å per pixel in the red, 4 Å in the blue. Taken through rather large apertures and calibrated on the AB79 scale by subdwarf G stars, the continuum fluxes agree well with those from the MCSP. Using such apertures results in imperfect sky subtraction (for [O I]) and poor correction for extinction in the O_2 band. The exposures provided about 10^4 counts per pixel near the emission triplets; the triplets appear the same in all spectra. After studying the individual spectra, we added the four available to provide mean fluxes. Figure 3 shows these co-added spectra; the noise is low, which is fortunate, since the lines are weak. We have the flux in the continuum near the emission lines on an absolute scale; we compute absolute emission-line fluxes by dividing the observed mean fluxes including emission by a smooth continuum. We consider later the effect of possible underlying absorption at Hα. The Balmer decrement is unusually flat, and $F(\text{H}\alpha)/F(\text{H}\beta)$ differs from the optically thin recombination value by a factor near 5, as noted in Greenstein (1983).

We have only a time-averaged spectrum and magnetic field if the star rotates rapidly. Within the 3 months of the 1982 observations the emission-line wavelengths appear constant. Schneider and Gunn kindly provided us with one PFUEI spectrum 10 months later, at 10 Å per pixel, which shows the same triplet structure as in 1982 in both Hα and Hβ. The separation of the σ_- and σ_+ peaks of Hα is 433 Å versus 453 Å on the DBSP. Hence there is some evidence that the magnetic field and the strength of emission are constant on moderate time scales.

IV. EMISSION-LINE DATA ANALYSIS

To determine the wavelength centroids and equivalent widths of the Zeeman triplet components, each reduced spectrum was first flattened and normalized to unity in the continuum. Selected continuum points far to the red and blue of Hα and Hβ emission lines were fitted by a spline in order to define the continuum level at the emission features. No underlying hydrogen absorption was noted outside the Zeeman-split emission. In Hα, the flux between the central (π) and blue (σ_+) components is a few percent above the continuum level (see the spectrum of Hα in Fig. 3). We discuss in § VI the effect of possible underlying Hα absorption concealed by the emission. The spline placement at Hβ, however, is quite uncertain: (1) it lies near the edge of the wavelength region covered by the blue CCD; (2) the continuum spectrum seems to be "curved"; (3) emission Hγ may exist. The Balmer decrement is less well determined than we might have expected.

With the individual spectra normalized as described, each line profile was approximated as Gaussian and fitted by a function of the form

$$f(\lambda) = A \exp -[(\lambda - \lambda_c)^2/2\sigma^2] . \quad (5)$$

Individual spectra are consistent with the positions λ_c and strengths A being constant. The four spectra were added, and then the summed spectrum was flattened and fitted with Gaussian profiles. This final representation of the features appears in Figures 4 and 5 and numerically in Table 1. The amplitude A is negative in emission, and we use its absolute value. The area of a Gaussian of the form of equation (5) is $W = (2\pi)^{1/2} A\sigma$; using the results from the summed spectra and the MCSP continuum fluxes near Hα and Hβ, we obtain the absolute emission-line fluxes. These give the atypical Balmer decrement $F(\text{H}\alpha)/F(\text{H}\beta) \approx 0.73$. After correction for underlying absorption lines, the corrected flux and luminosity, $L(\text{H}\alpha)$, are given in Table 4.

© American Astronomical Society • Provided by the NASA Astrophysics Data System

1985ApJ...289..732G

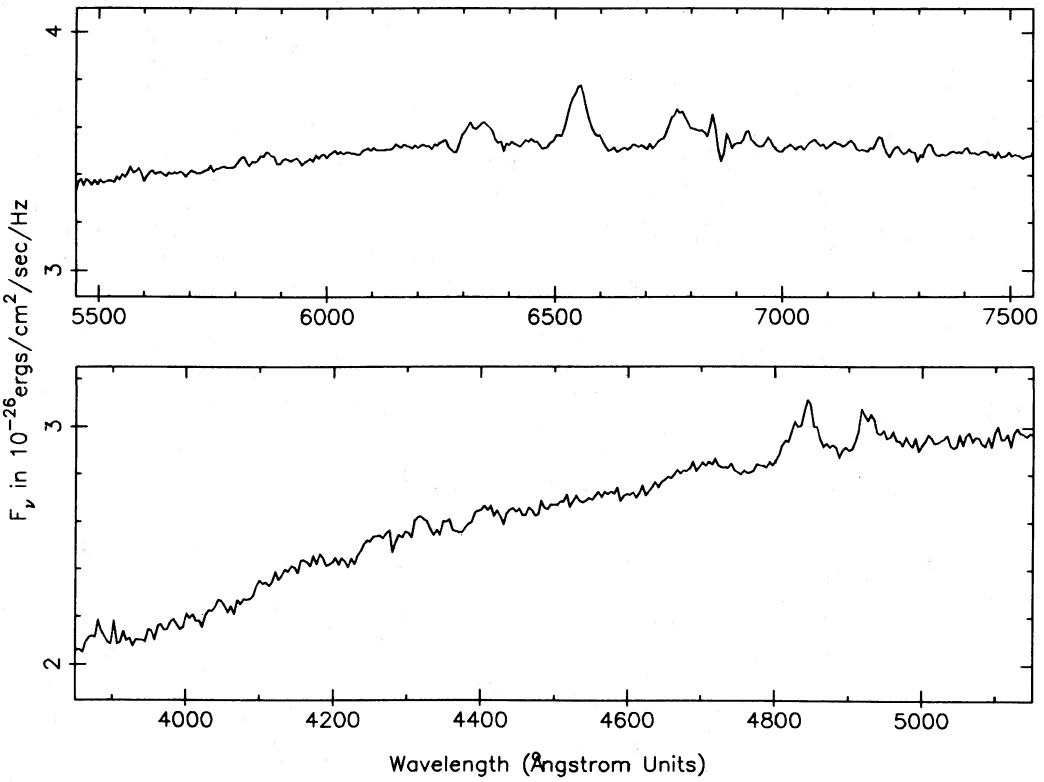


FIG. 3.—*Top*, mean fluxes in GD 356 from four CCD spectra; units are mJy. Note the low noise (~0.03 mJy). Anomalies near 6850 Å arise from incomplete correction for the atmospheric B band. No trace of broader, stellar, underlying Hα absorption is seen, but the Zeeman emission triplet is conspicuous. *Bottom*, the Hβ emission triplet is less symmetric than Hα; weak complex Hγ emission may be superposed on the decreasing ultraviolet continuum. The complexity and curvature of the continuum makes fitting the background with a spline quite uncertain.

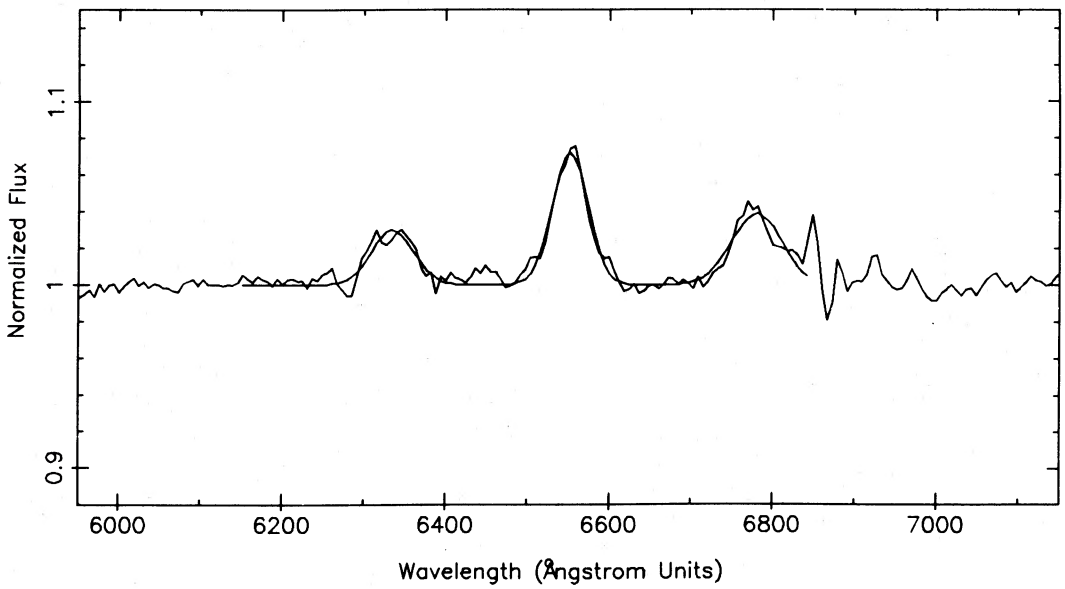


FIG. 4.—The continuum has been flattened and normalized to unity with a spline with Gaussians fitted to the Hα Zeeman triplet (data in Table 1). The splitting is ±220 Å, with little asymmetry from the quadratic Zeeman effect.

© American Astronomical Society • Provided by the NASA Astrophysics Data System

1985ApJ...289..732G

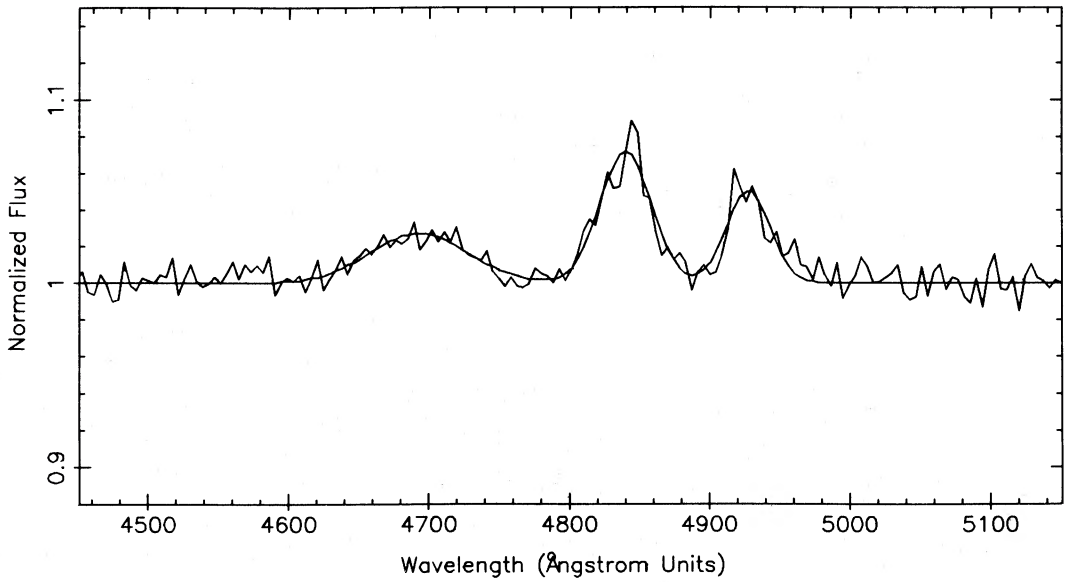


FIG. 5.—The continuum has been flattened and normalized with Gaussians fitted to the Hβ emission triplet (data in Table 1). The σ_+ component is broad. The asymmetry of the quadratic Zeeman effect shifts the σ components to +90 Å and −150 Å.

V. FITTING MODELS TO THE DATA

In order to determine the physical parameters of the region producing this Balmer emission, we first assumed it to be an extended corona-like volume surrounding a white dwarf (a model often used for thermal X-ray stellar sources). The radius of the star, $R_* = 6.8 \times 10^8$ cm, was taken as the unit of length, with the corona extending a few R_* outward. We assumed that a geometrically small, centrally located dipole was embedded, so that if the surface value of the polar field B_p is given, the field intensity at the point described by spherical polar coordinates (r, θ, ϕ) is given by

$$|\boldsymbol{B}| = B_p(R_*/r)^3(0.25 + 0.75 \cos^2 \theta)^{1/2} . \quad (6)$$

The density and temperature were assumed to be functions only of the radial coordinate, r. At each cell in a grid around the star, the emission was calculated, using the absolute value of the field, from

$$j_\nu = N_n(N_e, T)A_{n2}(B)h\nu_{n2}f(\nu - \nu_{n2}) . \quad (7)$$

Here, $f(\nu - \nu_{n2})$ represents a normalized line profile (in actuality the instrumental profile) for each Zeeman component. $A_{n2}(B)$ is the Einstein transition probability in a magnetic field of strength $|\boldsymbol{B}|$ for the line with upper quantum number n. Strengths are from Tables I and II and equation (9) of Kemic (1974). The quantity $N_n(N_e, T)$ is the number density of atoms in the upper state as a function of electron density and temperature. These number densities were calculated under several different assumptions concerning the density regimes and with different astrophysical approximations: (i) LTE, (ii) case A recombination (Baker and Menzel 1938), (iii) case B (Pengelly 1964), (iv) a non-LTE high-density slab approximation (Drake and Ulrich 1980). Case iv requires optically thick Balmer lines and may not be applicable. In cases ii–iv a spline interpolation was used on data from published tables to determine the factors b_{nl} giving the population for each sublevel described by (n, l), in the relevant density regime, assumed unaffected by the field:

$$b_{nl} = N(\text{NLTE})/N_n(\text{LTE}) . \quad (8)$$

These are relative to the N_n(LTE) calculated from the Saha and Boltzmann equations; theoretical values of b_{nl} are taken from the references cited above. Finally, the volume emissivity was found by summing equation (7), with each Zeeman component centered on the wavelength in the tables computed by Kemic (1974). We ignored radiative transfer effects, self-absorption, and the angle between the field axis and the line of sight. These approximations are possible because the lines are optically thin and weak. To predict absolute fluxes, for a given volume and electron density, we assumed a compromise standard distance, $d_* = 40$ pc. The uncertainty (discussed in § IX) arises from the question whether the star is overluminous, as a white dwarf, for the same reason that it is unique in having emission lines in a strong magnetic field. We adopt the standard white dwarf radius, $R_* = 6.8 \times 10^8$ cm. The electron densities derived for the tables scale downward by roughly a factor of 2 for the more probable distance of 20 pc, valid if the star has the same luminosity for its color as a normal degenerate.

A wide variety of fields and density laws tested for such corona-like models provided unsatisfactory fits to Hα. The parameters for one of the best of these models are given as model E1 in Table 2. The observed Zeeman patterns in Hα and Hβ show three quite widely separated Zeeman components; a typical coronal spectrum (as shown in Fig. 6*a*) predicted signifi-

TABLE 1

PROPERTIES OF GD 356 EMISSION

λ	A	σ	W	ΣW	AB (cont.)
Gaussian Fits to Hα Emission					
6335.....	−0.032	25.9	2.09	...	...
6552.....	−0.077	21.9	4.24	9.6 ± 10%	14.97
6780.....	−0.042	31.0	3.27	...	...
Gaussian Fits to Hβ Emission					
4692.....	−0.027	35.2	2.38	...	...
4839.....	−0.072	18.5	3.31	7.7 ± 15%	15.05
4927.....	−0.050	15.6	1.96	...	...

© American Astronomical Society • Provided by the NASA Astrophysics Data System

1985ApJ...289..732G

TABLE 2

MODEL PARAMETERS FOR EMISSION IN GD 356 (T_{el} = 20,000 K)

Designation	B_p (MG)	log N_e	log N(H I)	Thickness	Remarks
E1.....	22	11.15	2.99	extended	Large corona; dipole
E2.....	22	11.56	var.	$0.4R_*$	Limited corona; cutoff $1.4R_*$; $T_{el} = (1/r)^2$; dipole
E3.....	20	14.2	9.1	$10^{-4}R_*$	Chromosphere; dipole
E4.....	11.2	13.65	7.99	$10^{-4}R_*$	Chromosphere; random fields; $\sigma(B)$ = 1.37 MG

cant emission flux between these three components. The emission flux at small displacements from the π component arises in regions of lower magnetic field ($R \geq 2R_*$). We could match the observed spectrum better by assuming a sharp radial density cutoff, or a temperature distribution such that only neutral hydrogen exists beyond radius R_t. Observed profiles limited the cutoff to one which gave a field strength not too far below B_p, at $R_* \leq R_t \leq 2R_*$. Data for such a model are shown in Table 2 model E2); the resulting emission is plotted in Figure 6*b*. Various combinations of R_t and power-law temperature distributions were tried, and they provided fits of similar quality. We believe that such models are unrealistically complex and that the resulting fits to the data are contrived. The second shortcoming of corona-like models was their steep Balmer decrement. Only moderate electron densities ($N_e \approx 10^9$ cm^{-3}) follow if the volume, V, is large, the observed flux having fixed the value of $N_e^2 V$. As a result, model parameters which matched the observed Hα gave insufficient flux at Hβ (see Fig. 6*c*).

We replaced the corona by a thin-shell model, which we call a chromosphere. We adopt a 20,000 K electron temperature and a shell of thickness of $10^{-4}R_*$. In the chromospheric models the much smaller volume requires higher N_e and produces a flatter Balmer decrement. The shell gives negligible radial dependence of field strength, only the factor of 2 dependence on magnetic latitude (eq. [6]). We can neglect the dependence of the predicted emission profile on the angle between the line of sight and the magnetic pole (which we will call α) because the optical depth is small and we have neglected radiation transfer. Figure 7*a* shows how theoretical contributions to the total line profile add in predicting the Zeeman structure. The lowest field shell (magnetic equator) produces the innermost short-wavelength peak of the σ_- component and the innermost long-wavelength peak of the σ_+ component. In the π component, only the highest field shell is affected by the quadratic shift. In Figure 7*b* the fit to Hα is at a polar field of 20 MG, and log N_e = 14.2, with data in E3 of Table 2. The thickness is kept small; the scale height for a white dwarf isothermal chromosphere is $\sim 10^4 A^{-1}$ cm for atomic weight A. In both Figures 7*a* and 7*b*, little flux is predicted or observed between the σ and π components; the theoretical fit is acceptable. There is a subjective element in choosing the best fit shell model, but we believe we can exclude B_p as low as 10 MG. Such a field is unacceptable, leaving too little empty space between the three components. The observed wavelengths of the Gaussian fitted to the data (in Table 1) are matched by the centroid of the theoretical components at a B_p near 20 MG.

The same shell model, when applied to Hβ, predicts lines at the observed wavelengths but too weak by factor of between 2.5 and 3.0. We scaled $N_e^2 V$ upward by 2.7 to compare the emission with the data on Hβ. This high-density model (log $N_e \geq 14.2$) is optically very thick in Lyα ($\tau \approx 10^4$). We need that high a τ to flatten the Balmer decrement as much as possible if we try to match (even approximately) the observed line ratios. At high density we used population numbers from models of hydrogen-emitting regions, optically thick in Hα and Lyα, computed by Drake and Ulrich (1980), even though an optically thick Hα line should be strong. Magnetic broadening reduces the optical depth in the line of sight, for a given number of atoms, to an extent which depends on the unknown linear scale over which changes in field occur. Others have computed extreme models for the dense emission-line regions of quasars. Elitzur *et al.* (1983) proposed a more unusual model for cataclysmic variables; they use a strong, power-law radiation field near an accretion disk to strengthen higher-n Balmer lines and further weaken Hα. Their F(Hα)/F(Hβ) drops to 0.6 (well below our value) for a large excess of UV radiation. We lack evidence for excessive UV and have no observed X-ray flux; their predicted shallow Balmer decrement is closest to what we observe.[1]

There is an interesting difference between conditions in GD 356 and in disk or quasar emission-line regions in the intrinsic line width, and its source. The strong magnetic field splits or broadens high Balmer lines increasingly. Even for $n = 3$, the splitting in Hα is near 10%. A field variation of 10 MG along a line of sight corresponds to $v/c \approx 0.01$. While we may neglect the complex radiation transfer effects in the line in a strong field, we must and have included the corresponding line widths in computing optical depths in lines. We can provide a first-fit model because the small optical depths in the observable lines minimize the transfer effects. This is not true for Lyα; the polarization in the lines will also provide theoretical difficulties. In a further attempt to explain the shallow Balmer decrement, we turn to the effect of possible underlying Hα absorption.

[1] Factors in computing the flux in an emission line have errors. The decrement is

$$\frac{f\alpha}{f\beta} = \left(\frac{\Sigma W\alpha}{\Sigma W\beta}\right)\left[\frac{f(\text{cont})\alpha}{f(\text{cont})\beta}\right]\left[\frac{(dv/d\lambda)\alpha}{(dv/d\lambda)\beta}\right].$$

The product of the last two terms in square brackets is 0.59; the ratio of equivalent widths, as plotted in the figures is 1.25 $\pm$ 0.05. The ratio of fluxes in the lines is then 0.73 $\pm$ 0.13. Experimentation with spline fitting shows that the errors in $W\alpha$ arise mostly from vertical shifts in the background, with 10% a fair representation of the error. The curvature of the continuum near Hβ and the absence of undisturbed continuum result in a possible further reduction of $W\beta$. But even combined with the plausible highest value of $W\alpha$, the ratio of fluxes is less than unity. The errors cannot be large enough to fit the low-density recombinatiion theory. The flux received from the Zeeman emission triplet is $f\alpha = 2.50 \times 10^{-14}$ ergs cm^{-2} s^{-1}; at the standard distance $d_* = 40$ pc, the luminosity $L\alpha = 4.77 \times 10^{27}$ ergs s^{-1}. At Hβ, the corresponding numbers are 3.39×10^{-14} ergs cm^{-2} s^{-1} and 6.46×10^{27} ergs s^{-1}.

© American Astronomical Society • Provided by the NASA Astrophysics Data System

1985ApJ...289..732G

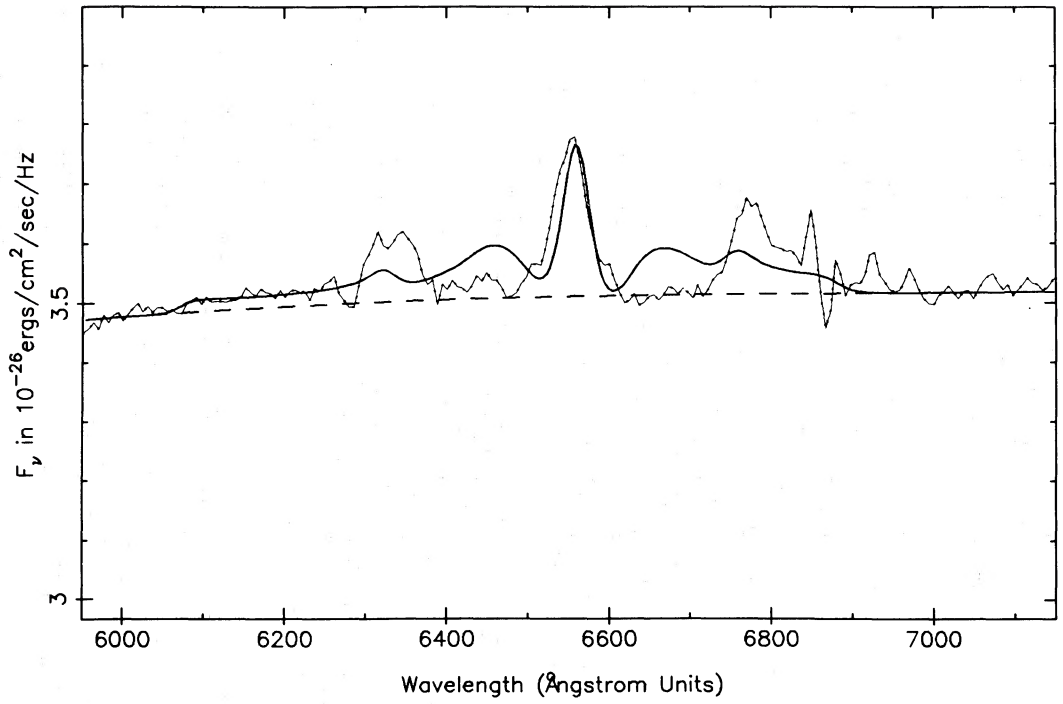


FIG. 6a

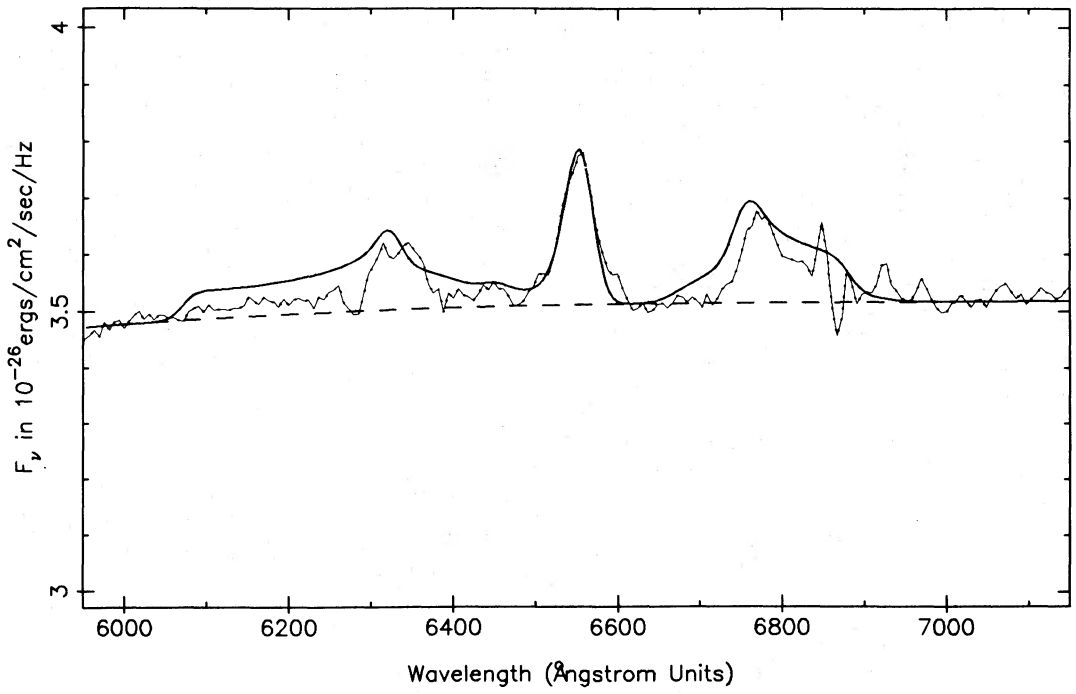


FIG. 6b

FIG. 6.—(*a*) A dipole magnetic field in an isothermal homogeneous corona (data in Table 2, E1) produces the predicted Hα emission shown by the smooth line, which is a poor fit to the GD 356 data (*jagged line*). The gas at large distances contains magnetic field well below the field's polar value, B_p, of 22 MG, producing emission at small displacements. In such a model the gaps between the π and σ components are filled in. (*b*) In an ad hoc coronal model, a radial temperature cutoff (see Table 2, E2) has been introduced to reduce the ionization and recombination beyond $1.4R_*$. The fit to the observed Hα emission is a possible one. The polar field is $B_p = 22$ MG. (*c*) Using the truncated coronal model, E2, of Fig. 6*b*, the predicted Balmer decrement is too steep, and the Hβ emission too weak. Even the wavelength agreement is poor.

© American Astronomical Society • Provided by the NASA Astrophysics Data System

1985ApJ...289..732G

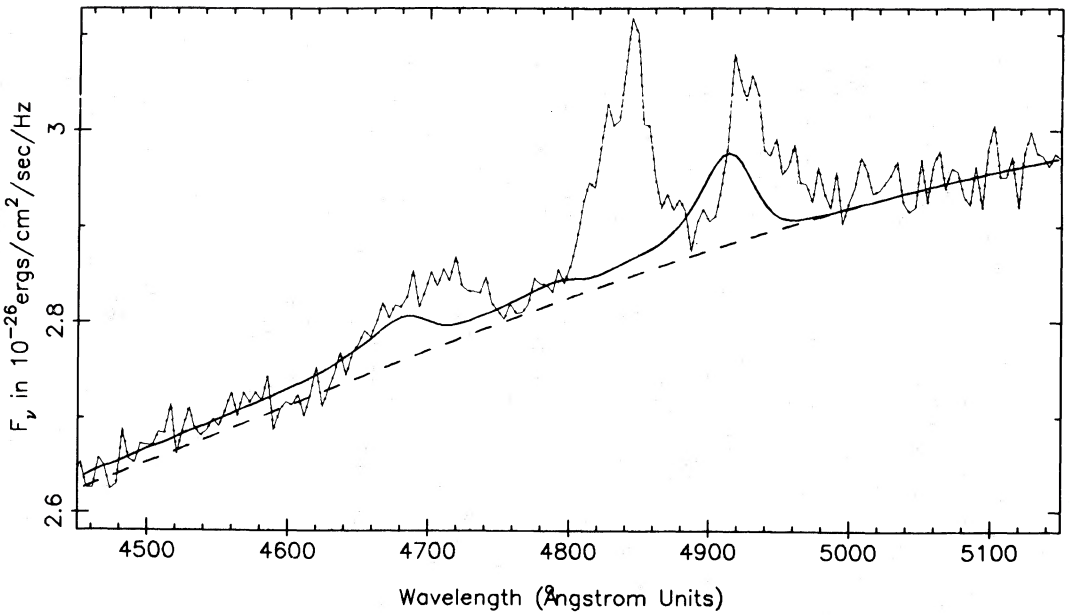


FIG. 6c

VI. HYDROGEN ABSORPTION IN A MAGNETIC DEGENERATE, G99-47

To reconstruct the flux in GD 356 on which the Hα emission-line triplet is superposed, we find guidance from available spectra of the cool magnetic degenerate G99-47 (0553+05, Gr 290, type DAP9). This star is notable for the presence of the Zeeman triplet of Hα in absorption and for the polarization discussed by Liebert, Angel, and Landstreet (1975, hereafter LAL). In LAL, the signal-to-noise ratio is such that only the π component is seen in their flux output; however, the associated wavelength dependence of the polarization is conspicuous in their data. They see the π component at 6542 ± 5 Å, with 2.5 Å equivalent width. We have two good Palomar DBSP CCD spectra at Hα and one at Hβ with excellent signal-to-noise ratio. The sum of the red spectra is at the top of Figure 8; the bottom shows the blue spectrum, averaged over three pixels (12 Å) to improve the signal-to-noise ratio even further. The absorption triplet seen resembles the emission triplet in GD 356, so we use the G99-47 absorption to model the invisible absorption that probably exists in the GD 356 atmosphere. We fit the continuum by a spline and the absorption lines by Gaussians using equation (5). The normalized fluxes are shown in Figure 9, with the Gaussian fits. The centroids are at 6251, 6546, and 6821 Å; the strengths and widths (see Table 3) are remarkably like those of the emission fits in GD 356. The equivalent width in absorption is 7.8 Å, compared with 9.6 Å for the emission in GD 356. We can easily deduce that the mean field is near 15 MG in G99-47 from the Kemic (1974) tables using the observed wavelengths of Gaussians fitted to the absorption. The σ_+ and σ_- components are separated by 576 Å, less than the 680 Å predicted in LAL; however, our new determination seems reliable. The predicted separation of the σ components is 217 Å at 10 MG and 416 Å at 20 MG. We expect that Hβ is over 300 Å broad, and that its Zeeman components will be diffuse and invisible in G99-47. We expect this from stellar-atmosphere theory and from the fact that available CCD spectra show Hβ weak or absent in cool degenerates clearly showing Hα. A stationary dip near 4930 Å that might appear (between 10 and 20 MG) in the σ_- component of Hβ is not visible in Figure 8. The spectrum of G99-47 may best be described as "rough" near Hβ and possibly depressed by at most 3% over a region where, in contrast, GD 356 emission is strong at Hβ. See the Appendix for further study of the magnetic field in G99-47 and for the analysis of its polarization by Wickramasinghe and Martin (1979).

VII. THE CORRECTED Hα EMISSION IN GD 356

The data on G99-47 and their interpretation give us some idea, at least, as to the probable appearance of the underlying absorption line of Hα in GD 356. Since G99-47 is nearly 2000 K cooler, GD 356 could have stronger underlying absorption lines. The absorption profiles of G99-47 have about the same σ as the GD 356 emission. As a guide, we shift the centroids of the G99-47 absorptions to the wavelengths of the GD 356 emissions and normalize the spline fit to the continuum flux in G99-47 to agree with that in GD 356. At the top of Figure 10 we show the observed GD 356 emission lines and, downward from the same baseline, the shifted G99-47 absorption fit by suitable Gaussians. It is then possible to correct the observed GD 356 emission for the assumed presence of the absorption triplet in its reversing layer. We subtracted the assumed underlying absorption from the observed flux. After adding back the continuum spline and renormalizing (to facilitate further analysis), the result is as shown at the bottom of Figure 10. It is an emission profile strengthened by about 50%; the relative intensities of the σ/π components are preserved, and the individual components remain well separated. Were the G99-47 lines much wider, spurious wings would have been added. The

TABLE 3

GAUSSIAN FITS TO Hα ABSORPTION, G99-47

λ	A	σ	W	ΣW
6251.....	+0.040	28.7	2.86	...
6546.....	+0.063	13.0	2.06	7.85 ± 5%
6821.....	+0.049	23.0	2.93	...

© American Astronomical Society • Provided by the NASA Astrophysics Data System

1985ApJ...289..732G

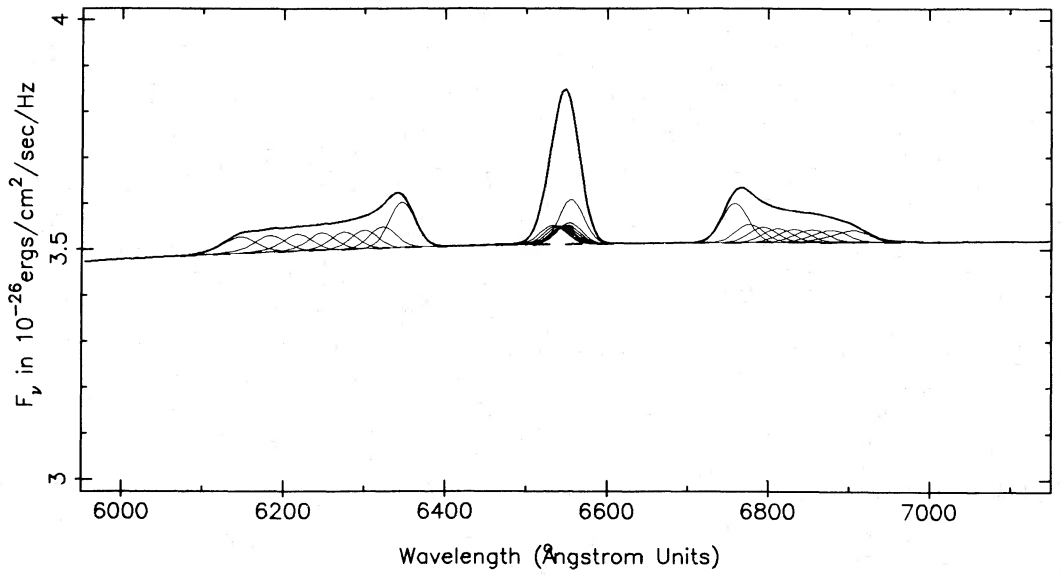


FIG. 7a

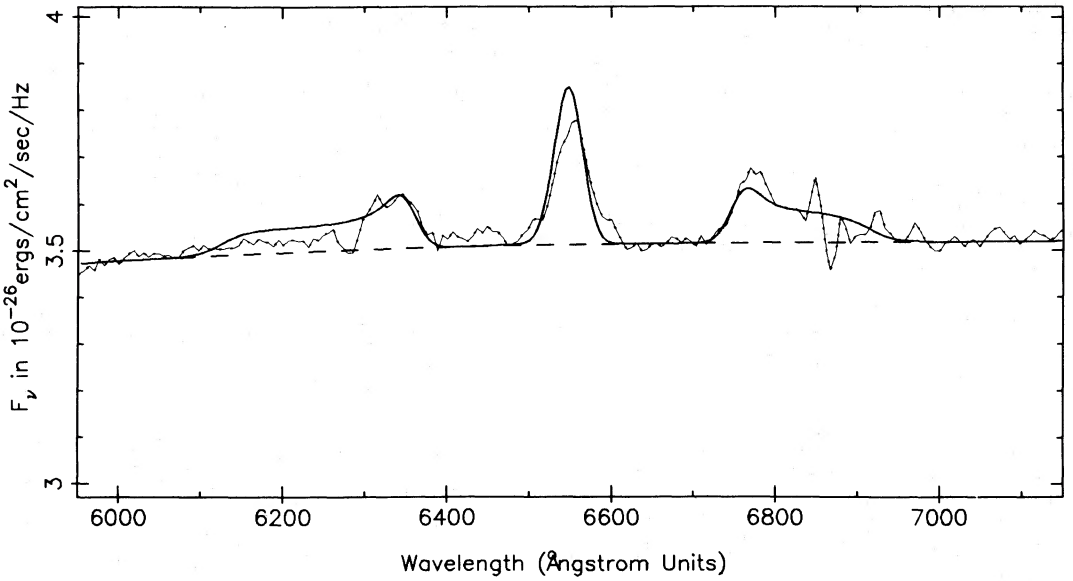


FIG. 7b

FIG. 7.—(*a*) In a chromospheric model (data in Table 2, E3) thin enough for the radial dependence of magnetic field to be negligible, the emission from eight individual shells of magnetic latitude is shown; the thick line is their sum. The optical depth of Lyα is large; $B_p = 20$ MG. The low field at the magnetic equator produces the emission peaks at the inner sides of the σ components. (*b*) The predicted line profile from the chromospheric model (Fig. 7*a*) fits Hα fairly well; there are clear gaps between the π and σ components. (*c*) The chromospheric model (Fig. 7*a*) must have its N_e^2 multiplied by 2.7 to give a strong enough Hβ. The emission-line fluxes require a flatter Balmer decrement than is provided even by high Lyα optical depth.

Gaussian fits to the corrected emission are given in Table 4A. The summed equivalent width (in units of nearby continuum) is 15 Å. Since no features were seen at Hβ in G99-47, correction merely results in an increase of the Hβ emission equivalent width of at most 3%. We cannot push the correction at Hα much further unless we explicitly assume that the invisible, underlying absorption triplet in GD 356 has a profile identical to the observed emission. We find the corrected final value $F(\mathrm{H}\alpha)/F(\mathrm{H}\beta) = 1.21$ rather than the 0.73 from the raw data. This not implausible ratio improves the agreement of the flat Balmer decrement with theories of high-density emission regions.

The effect of the correction of Hα is mainly to increase flux contrast and to produce somewhat narrower lines. These can be fitted either by a dipole in a thin chromosphere, essentially by scaling the optical depths by a factor of 1.5, or by a random distribution of effective fields. The line widths, measured by σ in Table 4A, are from 17 to 25 Å, less than in the raw data. Dipoles will fit the corrected data worse than they did in Figure 7. If the magnetic field were a small-scale tangled one, having an effective mean value and dispersion, we would have (to the extent that shifts are linear in field) a Gaussian distribution of wavelength shifts. In Figure 11 we present the final fit of such a Gaussian distribution of magnetic fields with a mean of

© American Astronomical Society • Provided by the NASA Astrophysics Data System

1985ApJ...289..732G

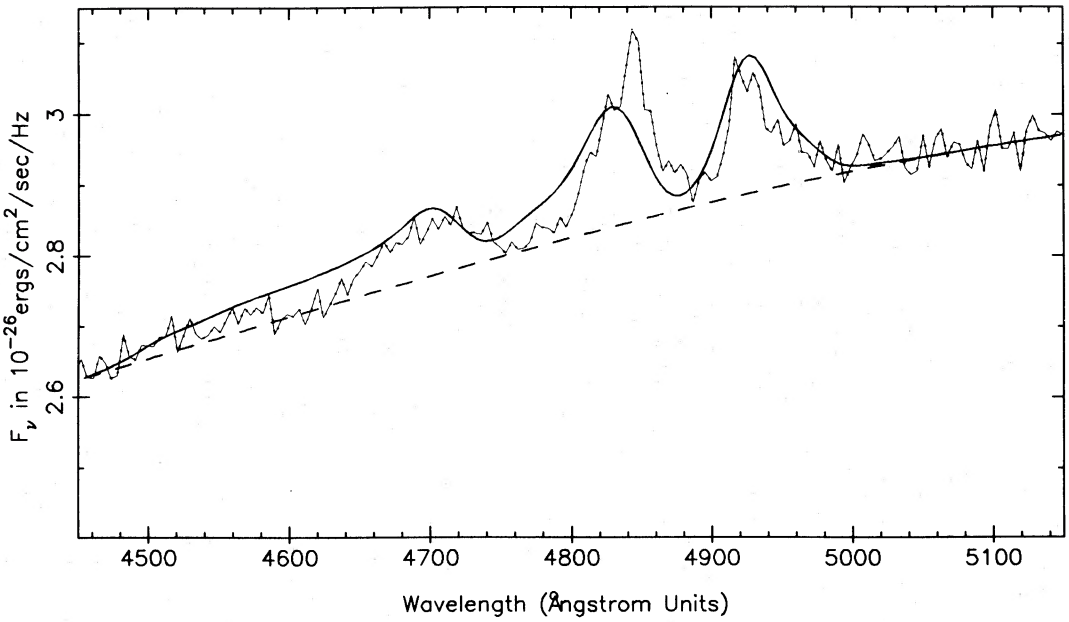


FIG. 7c

11.2 MG and a dispersion of 1.3 MG to the corrected Hα emission in GD 356. Parameters for this fit are E4 in Table 2 and in Table 4B; it has lower density and about one-half the fields typical of dipole models.

VIII. DISCUSSION AND SPECULATIONS

In analyzing the observational data we did not emphasize the significance of the width of the emission lines; we assumed that the instrumental resolving power was 35 Å (GD 356) and 25 Å (G99-47) when adding the individual Zeeman components produced at a given field in order to match the intrinsically narrow π component. Otherwise the predicted lines would have had a jagged appearance. These full widths at half-power correspond to Gaussian σ's of 21 and 15 Å. The spectographic instrumental profile is dominated by the size of the aperture. The spectrograph resolution is at worst 1.5 pixels, and had a 2″ slit been used, its projected width would have corresponded to 3.5 pixels, or 21 Å. Such a slit would probably

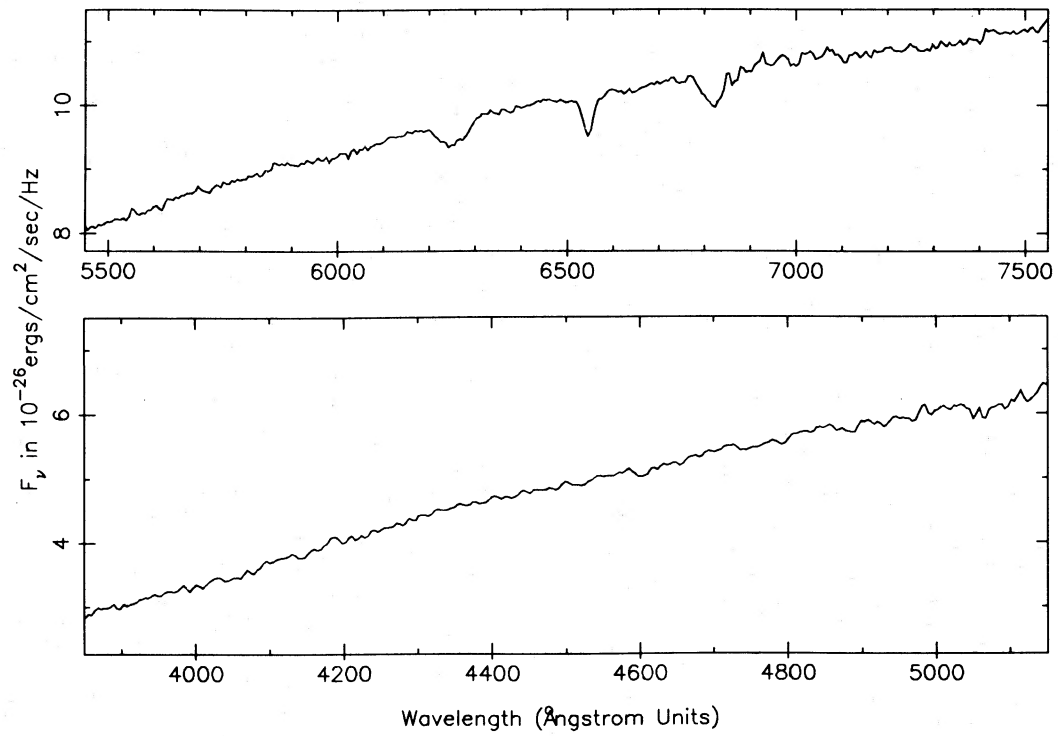


FIG. 8.—Fluxes in the cool magnetic degenerate G99-47 (from the sum of two CCD spectra) show the absorption triplet of Hα (*top*) clearly resolved, while Hβ (*bottom*), even when smoothed over three pixels, is invisible. The Balmer absorption decrement is steep.

© American Astronomical Society • Provided by the NASA Astrophysics Data System

1985ApJ...289..732G

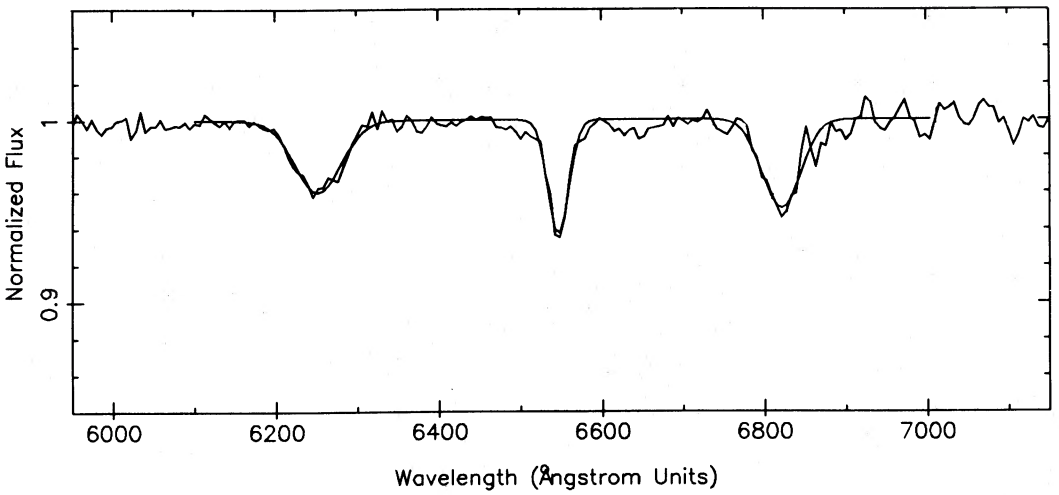


FIG. 9.—The Gaussian fit to the Hα absorption triplet in G99-47 is shown (from Table 3). In this strong field, the quadratic Zeeman effect is shown by shifts of −312, −17, and +258 Å from laboratory Hα.

yield a Gaussian of about 12 Å dispersion. But the spectra used were taken through round apertures (averaging 7″) to permit spectrophotometry. On two nights the seeing was estimated at 3″, on another 1″. It is difficult to assign an effective σ to the seeing disk, but at 2″, a range of FWHP of $12 \leq \sigma \leq 25$ Å is expected. The line width may not be purely instrumental in origin. Possible line-broadening sources in GD 356 are (1) velocity, (2) collision, pressure, or Stark, (3) magnetic field. If we take $\sigma_0 = (35^2 - 25^2)^{1/2} = 25$ Å, the Doppler velocity would be $v_0 \approx 1150$ km s^{-1}; this is 0.2 the velocity of escape, a reasonable motion in a low-density region such as occurs in solar prominences. However, in combination with the strong magnetic field, such large motions provide a potential for X-ray emission. Pressure and collisional broadening seem far too small to be important at our chromospheric densities; the linear Stark effect is inhibited by the strong magnetic field. There are five individual lines making up each Zeeman component. Each line has different $d\lambda/dB$ varying with B; if B is in MG, at 10 MG, $\langle |d\lambda/dB| \rangle = 3$ Å MG^{-1} for lines in the π component, 22 Å MG^{-1} for the σ_+ component, and 17 Å MG^{-1} for the σ_- component. If all components had equal strength, with $|\boldsymbol{B}| = 10$ MG, a plausible spread of 1 MG would broaden the σ blends by about 20 Å but contribute only 3 Å to the width of the π blend. Our tables show that most π component fits have Gaussians with $\sigma = 18$ Å, leaving its width as probably caused by the degraded resolution with large apertures. In those models where we adopted a dipole representation (with its factor of 2 variation in the field), the theoretical profiles were broader and more asymmetric than those observed. But with limited field variation (only 10%), in fits with Gaussian models, if there is an excess width, it might arise from an ordered Doppler velocity field.

TABLE 4

CORRECTED Hα EMISSION IN GD 356

A. GAUSSIAN FITS

λ	A	σ	W	ΣW
6334.....	−0.072	25.0	4.50	...
6552.....	−0.128	17.2	5.51	15.2
6782.....	−0.087	23.8	5.91	...

B. MODEL PARAMETERS FITTING CORRECTED EMISSION

$\langle B \rangle$	11.2 MG, $\sigma = 1.37$ MG
f(Hα)	3.96×10^{-14} cm^{-2} s^{-1}
L(Hα)	7.55×10^{27} ergs s^{-1}

Single white dwarfs are slow rotators, with v_R below 100 km s^{-1}. Unless there is an unseen companion (without the active accretion disk of a cataclysmic variable), we need an internal source of chromospheric motion. The normal hydrogen white dwarf at 8000 K has a convection zone, a thin nondegenerate envelope, and a hot degenerate core. The zone of partial hydrogen ionization becomes important at $\tau \geq 1000$. The density is much higher than in main-sequence convection zones, so the convective energy transport requires only low velocities. The velocities and their behavior as they approach the surface have not been determined; the density drops by 100 from $\tau = 10^3$ to $\tau = 10^{-4}$. Momentum conservation in stream motion requires only a tenfold velocity increase. If analogs of solar granules are produced on a white dwarf, would they have low velocities and small size? The scale height in a white dwarf upper atmosphere is $\sim 10^4$ cm, so that by analogy with the Sun, white dwarf granules would be small (~ 1 km) and last 1 s, if the velocity were as large as 1 km s^{-1}. Still, it is worth noting that the temperature gradient below is enormously steep and may produce effects measured by the scale height of the region between the surface and the degenerate core. This has a physical extent of $\sim 6 \times 10^{-3} R_*$, or 40 km, so that "granules" of that scale would have appreciable size; also, in that region, $\langle dT/dr \rangle \approx 2$ K cm^{-1}, which is 10^4 times steeper than in the Sun. As a speculation, assume that granules of moderate size can create acoustic waves at the top of the white dwarf atmosphere. If this still occurs in the presence of a strong magnetic field, there would be magneticacoustic heating of the chromosphere. The chromosphere would be above a temperature inversion, i.e., ionized gas "outside" the normal atmosphere. A referee kindly notes that severe distortion of the temperature structure of the "reversing layer" may be expected from the chromospheric radiation, so that the underlying absorption lines could be quite different.

Let us neglect the effect of the chromosphere on the photosphere to consider characteristics of the energy balance between gravitational, thermal, and magnetic energy. In an

© American Astronomical Society • Provided by the NASA Astrophysics Data System

1985ApJ...289..732G

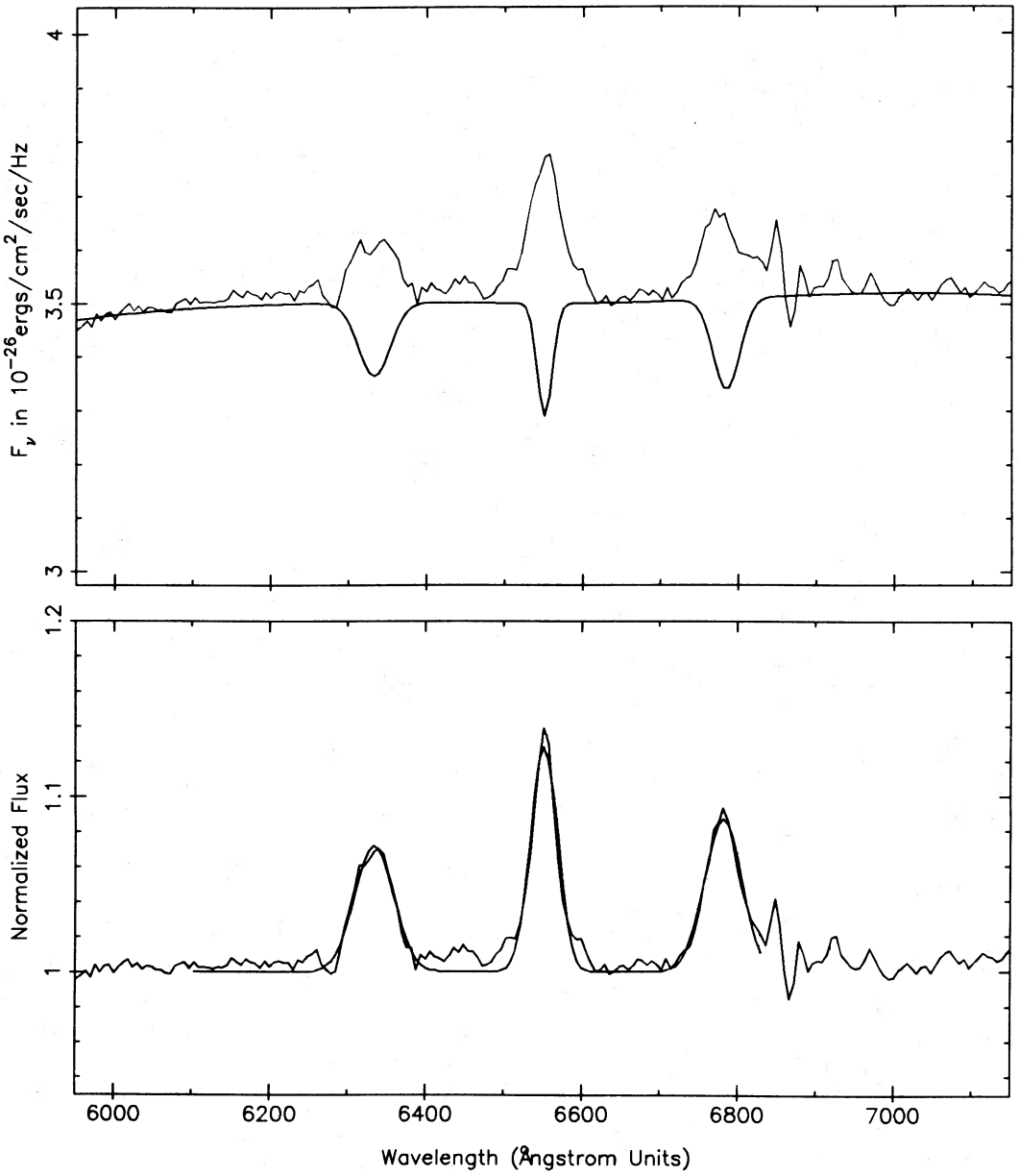


FIG. 10.—*Top*, the thin, jagged line is the observed spectrum of GD 356 (flattened with a spline). The smooth line is the Gaussian representation of the G99-47 data, after the components have been adjusted in wavelength to fit the GD 356 emission and after the continuum has been matched to GD 356. *Bottom*, the normalized flux in GD 356, after the observed emission fluxes are corrected upward in the amount of the smoothed absorptions in G99-47, shown at the top of this figure. These corrected emission fluxes are fitted by three Gaussians as shown; their summed emission equivalent width is increased by 50% in this method of correcting for an assumed underlying absorption.

ionized gas with field B_* in units of MG and N_{e*} in 10^{14} cm^{-3} (characteristic of our chromospheric models), the Alfvén velocity is

$$v_A/c = 0.73 B_* N_{e*}^{-1/2} . \quad (9)$$

Thus v_A is relativistic, the large magnetic energy dominating the motion of the charged particles. We may apply this to partially neutral matter in the star's reversing layer, if the electrons drag the neutral gas along. Detailed physical properties for a DA star of this temperature are available from a model-atmosphere computer printout from Koester (1978). We convert from the electron density to the total particle number and use the gas pressure and temperature via the gas constant R_g. Then in terms of the parameters given in the model,

$$\frac{v_A}{c} = \frac{B}{c}\left(\frac{R_g}{4\pi}\right)^{1/2}\left(\frac{T}{P_g}\right)^{1/2} . \quad (10)$$

Exploration of the DA model shows that at $\tau = 500$, $v_A/c = 0.015$ (matter 10% ionized); at $\tau = 1$, $v_A/c = 0.024$ (matter 1% ionized); at $\tau = 10^{-4}$, $v_A/c = 0.137$ (10^{-4} ionized). But in purely chromospheric models the ionization should be nearly complete, so that v_A/c is the much larger value given by equation (9). With a temperature inversion (we assumed $T_{el} =$ 20,000 K) and heating above the surface, concepts like

© American Astronomical Society • Provided by the NASA Astrophysics Data System

1985ApJ...289..732G

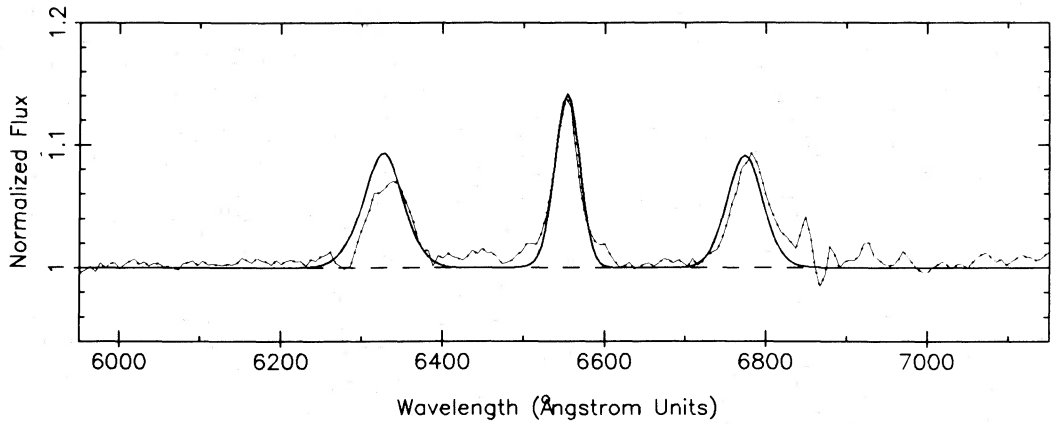


FIG. 11.—The flux in GD 356 after correction for absorption is shown by the jagged line. A random distribution of magnetic fields, $\langle B \rangle = 11.2$ MG, with $\sigma = 1.3$ MG, fits the observed Hα quite well.

reversing layer and chromosphere must blend at some small τ. If the magnetic lines of force penetrate the reversing layer to the convective zone, they may be subject to irregular, buffeting, propagating Alfvén waves, which will travel upward at increasing speed, emerging from the chromosphere, with high velocity in a chaotic field.

The high magnetic energy makes the kinetic energy from expected velocity fields seem small ($v_\infty/c \approx 0.02$). Comparing magnetic energy density, U_M, and gravitational energy, U_G, we have

$$U_M > U_G \quad \text{if} \quad \frac{B^2}{4\pi} > \frac{GM\rho}{R}, \tag{11}$$

a condition valid if $\rho \leq 10^{-5}$ g cm^{-3} for $B = 10$ MG. As in AM Herculis stars, the atmosphere at small τ and the entire nearby low-density gas are dominated by the magnetic field. But we must remember that some cool degenerates have magnetic fields (G99-47 has an even stronger field) without emission lines. It seems that an unrecognized peculiarity must still be invoked for GD 356; one possibility is an unseen companion. There could now be an ongoing episode of interstellar accretion whose flow buffets gas for which the lines of force provide mechanical support and ohmic heating. We estimate the magnitude of the required accretion; if the magnetic field permits accretion over a fraction η of the geometric target area of the star, and if $\dot{m}$ is the accretion rate in the absence of magnetic field, then $\dot{m}\eta v_\infty^2/2$ is the kinetic energy input. Assume this energy is converted with efficiency β, balancing the luminosity in the emitting hydrogen, which is in the amount γL. This gives

$$\dot{m} = 2\gamma L/\beta\eta v_\infty^2 . \tag{12}$$

We evaluate equation (12) for $L = 1.4 \times 10^{30}$ ergs s^{-1} and assume $\eta\beta = 0.01$; $\gamma = 0.035$ comes from the recombination rate (see below). Then $\dot{m} = 1.3 \times 10^{-12}$ solar masses per year. This is a rather high but not impossible value. It would be low if a companion existed to provide matter for accretion. We should remark that a rotating thin torus of emitting gas might possibly produce a triple emission line at Hα. But it would fail completely to give the correct wavelengths of the observed Hβ. There is little doubt that a magnetic field is producing quadratic Zeeman shifts. Any apparent resemblance to SS 433 is a red herring.

IX. ESTIMATES OF THE ULTRAVIOLET SPECTRUM AND THE DISTANCE

A few remarks should be made about the recombination rate and its consequences for the value of γ and the expected ultraviolet spectrum. From our measurement of the fluxes in Hα and Hβ, we can count the number of transitions into the $n = 2$ state. Assume now a standard distance $d_* = 20$ pc. Neglecting self-absorption in all transitions, the expected number of Lyα photons is 7.7×10^{38} s^{-1}. The luminosity in Lyα is 1.25×10^{28} ergs s^{-1}, which results in a Lyα flux of 2.6×10^{-13} ergs cm^{-2} s^{-1}. The actual intensity to be expected for the σ component depends on the line width in Hz, which should be dominated by the magnetic splitting. Whether the line is observable depends on the resolution of the *IUE* and on the magnetic line broadening. The geocoronal Lyα is uncomfortably close.

Computation of the splitting of the three components of Lyα is in Garstang (1977). At 100 MG, quadratic shifts are obvious; the splittings are -3576, $+5761$ cm^{-1}; at 10 MG they are -456, $+478$ cm^{-1}. The π component hardly moves. Interpolating for 22 MG (typical of our chromospheric models), we adopt $+15$ Å, placing the σ_- component near 1230 Å. If spread over the range from its undisplaced position to 1230 Å, its width is 3×10^{13} Hz, and the resultant flux is 0.8 mJy ($f_\nu = 8 \times 10^{-27}$ ergs cm^{-2} s^{-1} Hz^{-1}). Such a broad line has a predicted AB magnitude of 16.6. The line need not span the entire range of its Zeeman splitting. For example, if we adopt the random field model near 11 MG with dispersion of 10% of its mean, each component is only 1.5 Å wide. The AB magnitude would be 15.3 if the sharp σ_- component is at 1223 Å. This is unrealistic because a practical lower limit to the width is set by the *IUE* resolution. The σ_- component if at $\lambda \approx 1230$ Å should be resolved from the geocoronal line; if at 1223 Å, it might not be. Since the *IUE* resolution is near 4.5 Å, we predict AB = 16.5, even with the 11 MG random field. The estimate is independent of the distance. The computed numbers of recombinations in Hα and Hβ scale by $(d/d_*)^2$ as does the number of emitted Lyα photons. The inverse-square factor leaves Lyα flux and AB brightness unchanged at Earth. The change in distance will alter the $N_e^2 V$ deduced and therefore the N_e in our tables in a nearly linear manner.

There is another, more astrophysical, approach to predicting Lyα line strength. It yields a flux which depends on the actual distance but, unfortunately, involves knowing T_{el}. In all plausible "chromospheric" models, the flat Balmer decrement

© American Astronomical Society • Provided by the NASA Astrophysics Data System

1985ApJ...289..732G

requires the Lyα optical depth to be large. No account is taken of the transfer problem for Lyα photons as they diffuse out of the line core. Assume that the line is at least one *IUE* pixel wide. It emits over that one pixel as a blackbody at the chromospheric electron temperature. The explicit dependence of the f_ν of Lyα on T_{el} is given by the star's solid angle and the blackbody formula evaluated at that wavelength and T_{el}:

$$f_\nu = 2\pi h/c^2(R/d)^2\nu^3/[\exp(h\nu/kT_{el}) - 1], \quad (13)$$

$$f_\nu \approx 5.8 \times 10^{-43}[(R/R_*)/(d/d_*)]^2\nu^3/[\exp(h\nu/kT_{el}) - 1]. \quad (14)$$

Equation (14) gives the flux, in mJy, at the $[(R/R_*)/(d/d_*)]$ factor for the standard white dwarf, with $R_* = 6.8 \times 10^8$ cm and $d_* = 20$ pc. A flux of about 3 mJy is predicted if T_{el} is near 15,000 K and the line is optically thick. However, the dependence on T_{el} is steep; the fluxes are 23 mJy (at 20,000 K), 5 mJy (16,000 K), 0.4 mJy (12,000 K). Evaluating the flux at the Lyman limit (1 rydberg) gives 8 mJy (20,000 K) and 1 mJy (16,000 K). If the chromosphere is hot ($T_{el} \approx 20{,}000$ K), the Lyman continuum affects the energy balance. But Lyα is probably detectable with the *IUE* if the chromosphere is even warm.

In our discussion and tables we adopted a fixed radius and distance; the solid angle factor may need correction if the parallax is different and the star is not a normal white dwarf. If it is normal, we take the maximum size as 0.01 $R_\odot$ radius; the MCSP color-luminosity relation then predicts $M_V = 13.34$. With $V = 15.05$, the distance is 22 pc. However, if an accretion region exists, the luminosity might be higher. The nominal distance used in computing electron densities for the tables was $d_* = 40$ pc. This corresponded to $M_V = 12.04$, a conpromise between 13.3, predicted by the MCSP colors, and a possible brighter value such as might occur if GD 356 were overluminous for the same reason that makes it have emission lines.

White dwarfs with composite colors are measured too red and ascribed too faint an absolute magnitude (Greenstein 1984). But we dismissed in § II the possibility of the color being strongly affected by a companion. We consequently find the distance given by the blackbody law, i.e., from the absolute surface brightness at a selected wavelength, the V magnitude at 5400 Å. We look for that blackbody for which an assumed temperature and radius matches V. Since we know that the blackbody energy distribution fitted the MCSP data over a wide range of wavelengths (see Fig. 2), fitting the V magnitude gives an overall fit. The flux corresponding to AB = 15.05 is 3.5 mJy. Assume the radius unchanged, i.e., $R = R_*$ in equation (14), then $d = 22$ pc (for 8300 K), and $d = 20$ pc (for 8000 K). Thus, the use of a blackbody of reasonable temperature confirms the distance given by the MCSP colors as calibrated by white dwarfs of known parallax. A hydrogen model atmosphere at 7500 K would almost certainly give the same result.

We expect no detectable stellar ultraviolet flux from the blackbody near 8000 K or 8300 K; the ultraviolet flux from the hot portion of an accretion disk, if one exists, might be observable. Chromospheric emission might be seen in favorably located, optically thick ultraviolet lines at lower frequencies, where the blackbody flux at T_{el} is higher. The small distance used here makes parallax measurement important; the combination of uncertainties of both T_{el} and distance may be unraveled if additional chromospheric lines are found.

In conclusion, the Zeeman emission triplets of hydrogen in a strong magnetic field in GD 356 may be explained by a thin layer of high-density ionized gas, probably heated by the field. GD 356 seems to be unique. If the field is that of a dipole, its polar value is near 20 MG. The observed small polarization of the continuum (Angel, Borra, and Landstreet 1981) was $0.01\% \pm 0.05\%$; although based on only one observation, it is small for 20 MG. Depending on the inclination, one might expect about 0.5% continuum polarization. No attempts have yet been made to measure the polarization across Hα and Hβ. It is difficult to have the magnetic field confined only to a chromosphere. The required magnetic field has a mean of 11 MG, with 10% dispersion, if it has a small-scale, rather than dipole, geometry.

The gas may come from the white dwarf through a convective instability interacting with the magnetic field. If the origin of the gas is external, there may be either a still undetected companion or ongoing accretion of interstellar matter. Observations of parallax, high-resolution polarization, Lyα, and X-rays are needed, and should give further important clues. GD 356 affords prospects of important new insights on magnetic fields in dense stars and on ultraviolet or X-ray emission from their chromospheres or coronae.

This investigation was supported in part by a grant, 83-AST-05504, from the National Science Foundation to J. L. G.; J. K. M. is grateful for the support of a National Science Foundation Graduate Fellowship.

APPENDIX

Since the absorption-line profiles in G99-47 are now observed with much better signal-to-noise ratio than any previously published, we believe them worth detailed discussion. Our program for computing emission lines in a chromosphere contains the detailed Zeeman patterns derived from Kemic (1974), including the relative strengths. We use an elementary, linear radiative transfer approximation since the lines are weak. We scale the effective number of atoms (in LTE) in level $n = 2$ until the central absorption depths are correct. The distribution of optical depths with wavelength, from various zones of different magnetic latitude in a dipole field, was then computed. It resembles that shown (for emission lines) in Figure 7*a*. The field in G99-47, as shown by its absorption lines, is stronger than that in the emission-line region of GD 356. To predict the absorption spectrum from the optical depths, we must allow for limb darkening and for the angle α between the magnetic pole and the line of sight. We explored this problem and show some results in Figure 12. Data for these are in Table 5 (models A1, A2). To best represent the observed absorption lines, we find $B_p = 27$ MG if $\alpha = 90°$ and 16 MG if $\alpha = 0°$, although neither fit is good. Contributions to the line arise from a wide range of field strength. Only the strongest parts of such lines would be observed, so that the apparent relative strengths of the σ and π components would be anomalous. While the transfer theory is elementary, we doubt that its improvement would change the predicted line profiles radically.

Another, although nonphysical, descriptive model for absorption and emission lines may be tested. One may doubt the realism of a centred dipole of negligible extent in a white

© American Astronomical Society • Provided by the NASA Astrophysics Data System

1985ApJ...289..732G

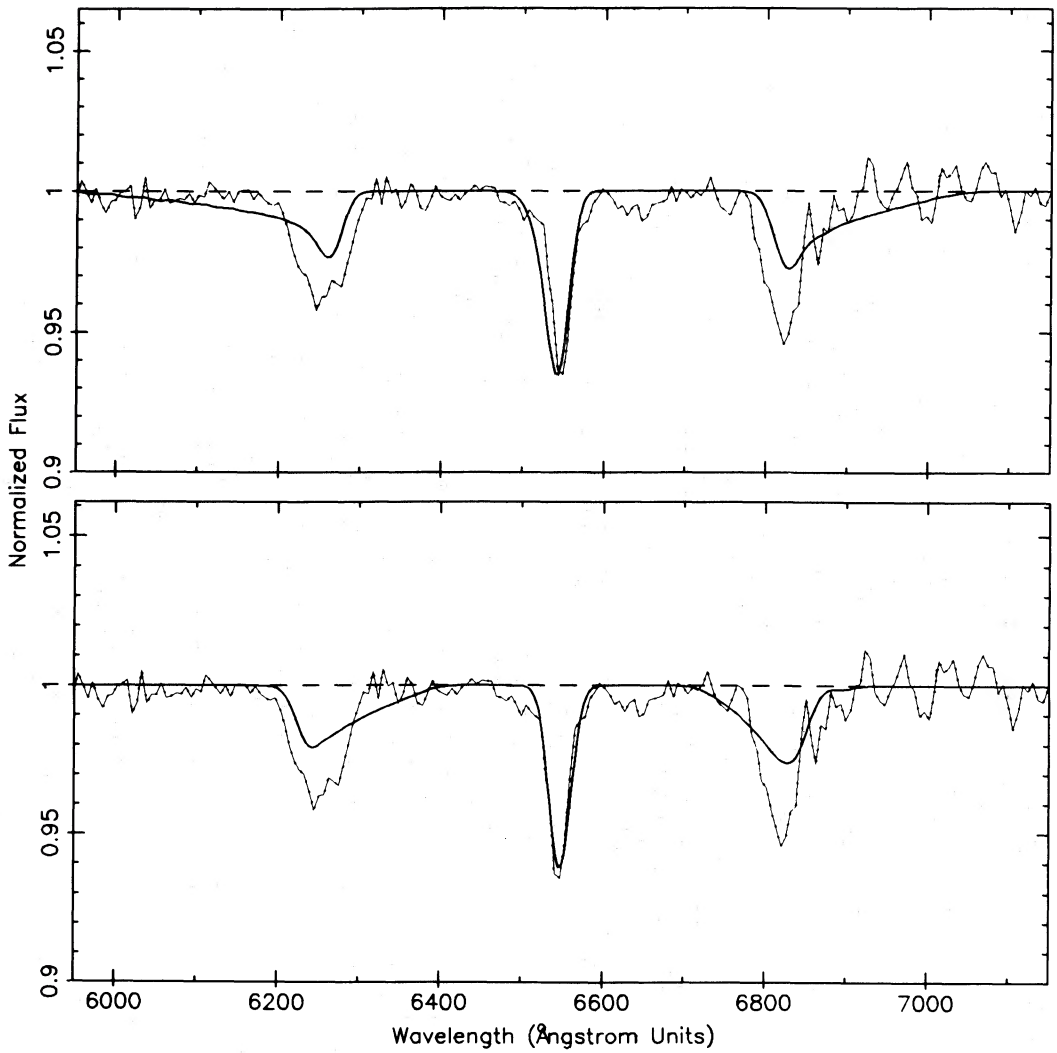


FIG. 12.—Fits of the Hα data for G99-47, a cool degenerate star, with a dipole field. Data in Table 5. *Top*, model A2: $B_p = 27$ MG, magnetic pole in the plane of the sky, i.e., $\alpha = 90°$; the central component is displaced, and wings become too broad in regions with large field. *Bottom*, model A1: $B_p = 16$ MG, with the pole in the line of sight, $\alpha = 0°$; regions of small field fill the space between the π and σ components.

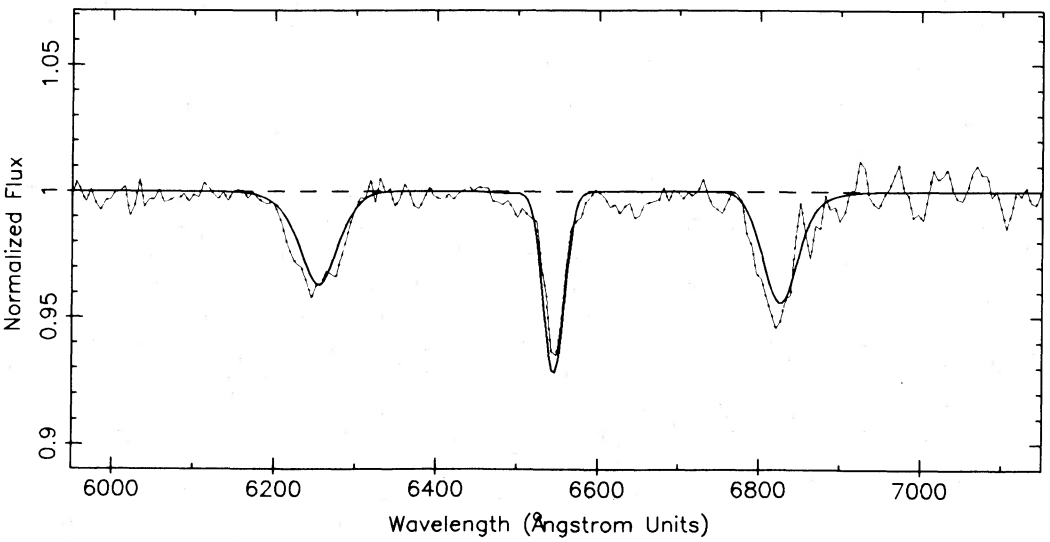


FIG. 13.—The observed Hα in G99-47 is fitted by a random distribution of small-scale fields, with $\langle B \rangle = 14$ MG, $\sigma = 1.4$ MG. Data in Table 5, A3. Line profiles and relative intensities are well matched.

© American Astronomical Society • Provided by the NASA Astrophysics Data System

1985ApJ...289..732G

TABLE 5

MODEL PARAMETERS FOR ABSORPTION IN G99-47
(T_{el} = 7500 K, LIMB DARKENING = 0.6, THICKNESS = $10^{-4}R_*$)

Desig.	B_p (MG)	log N_e	log N(H I)	α (°)	Remarks
A1.....	16	12.21	15.36	0	Dipole, latitude dependence
A2.....	27	12.21	15.36	90	Dipole, latitude dependence
A3.....	14	11.88	10.95	...	Random fields; σ = 1.36 MG

dwarf. The degenerate core has high electric conductivity; the nondegenerate envelope is convective at low T. Instead of a general poloidal field, there may exist fragments of twisted toroidal fields, accompanied by complex, possibly time-variable, surface fields of mixed polarity. Young, Schneider, and Shectman (1981) used a Gaussian distribution of $|\boldsymbol{B}|$ to fit the absorption lines seen in the magnetic white dwarf in AM Herculis (at low state). We may then neglect limb darkening and magnetic field orientation when predicting absorption lines. To compute the optical depths, we calculate each Zeeman component from a Gaussian distribution of fields with a given mean and dispersion. In Figure 13 we show how well $\langle|\boldsymbol{B}|\rangle$ = 14 MG, σ = 1.4 MG represents Hα in G99-47. Since each of the observed lines was approximately symmetric and well resolved, a Gaussian distribution of line displacements describes the data well since it does not produce the wings coming from the relatively high or low fields present in a dipole. However, we should not overstress data from one type of observation (line profiles with still limited resolution) and disregard those obtainable from another, i.e., continuum polarization. Wickramasinghe and Martin (1979) studied the observed polarization, which is near 0.5%, and its wavelength variation. The polarization is in quite satisfactory agreement with their predictions for B_p = 25 MG and a proper orientation. They predict that Hβ will not be visible. But they did not give a sufficiently detailed profile of Hα to compare with our new data, which have a much higher signal-to-noise ratio than what was available to them. However, we know that the line splitting predicted by their dipole models must be near what we observed.

REFERENCES

Angel, J. R. P., Borra, E. F., and Landstreet, J. D. 1981, *Ap. J. (Suppl.)*, **45**, 457.
Baker, J. G., and Menzel, D. H. 1938, *Ap. J.*, **88**, 52.
Drake, S. A., and Ulrich, R. K. 1980, *Ap. J. (Suppl.)*, **42**, 351.
Elitzur, M., Ferland, G. J., Mathews, W. G., and Shields, G. A. 1983, *Ap. J. (Letters)*, **272**, L55.
Garstang, R. 1977, *Rept. Progr. Phys.*, **40**, 105.
Giclas, H. L., Burnham, R., Jr., and Thomas, N. G. 1967, *Lowell Obs. Bull.*, Vol. 7, No. 4.
Greenstein, J. L. 1983, *IAU Circ.*, No. 3823.
———. 1984, *Ap. J.*, **276**, 602.
Greenstein, J. L., and Oke, J. B. 1983, *Ap. J.*, **252**, 295.
Kemic, S. B. 1974, *JILA Rept.*, No. 113.
Koester, D. 1978, private communication.
Liebert, J., Angel, J. R. P., and Landstreet, J. D. 1975, *Ap. J. (Letters)*, **202**, L139 (LAL).
Luyten, W. J. 1979, *NLTT Catalogue*, Vol. **1** (Minneapolis: University of Minnesota).
McCarthy, J. K., and Greenstein, J. L. 1983, *Bull. AAS*, **15**, 1966.
Oke, J. B., and Gunn, J. E. 1983, *Ap. J.*, **266**, 713.
Oke, J. B., and Wade, R. A. 1982, *A.J.*, **87**, 670.
Pengelly, R. M. 1964, *M.N.R.A.S.*, **127**, 145.
Shipman, H. L. 1977, *Ap. J.*, **213**, 188.
Wade, R. A. 1979, *A.J.*, **84**, 562.
Wickramasinghe, D. J., and Martin, B. 1979, *M.N.R.A.S.*, **188**, 165.
Young, P., Schneider, D., and Shectman, S. 1981, *Ap. J.*, **245**, 1043.

JESSE L. GREENSTEIN and JAMES K. MCCARTHY: Department of Astronomy, Mail Code, 105-24, California Institute of Technology, Pasadena, CA 91125

© American Astronomical Society • Provided by the NASA Astrophysics Data System